Impact of the inundation occurrence on the deep convection at continental scale from satellite observations and modeling experiments

C. Prigent,[1] N. Rochetin,[2] F. Aires,[3,4] E. Defer,[1] J.-Y. Grandpeix,[2] C. Jimenez,[5] and F. Papa[6]

Received 26 May 2011; revised 15 September 2011; accepted 17 October 2011; published 24 December 2011.

[1] This study is an attempt to evidence the impact of the inundation occurrence on the deep convection at continental scale. Three sources of satellite observations are carefully analyzed over the tropics for 3 years: A multisatellite wetland extent and dynamics data set, a deep convective activity index derived from passive microwave satellite measurements at 85 GHz, and precipitation estimates. Although many other effects contribute to the variability in the convection (e.g., large-scale circulation and weather regimes), careful examination of the seasonal and diurnal variations of the satellite-derived information makes it possible to observe two distinct regimes. The first regime corresponds to regions where the inundation is not generated by local precipitation. There it is shown that stronger convection happens during the minimum of the inundation, with a marked diurnal cycle of the deep convective activity. Simulations with a single-column model are in good agreement with these satellite observations. First, calculations show that during the season of minimum inundation, hydrometeors are present higher in altitude, increasing the likelihood of larger ice quantities aloft. Second, the diurnal cycle of the convective activity related to the presence of large ice quantities has a larger amplitude. The second regime corresponds to regions where the inundation is directly generated by local precipitation. There our observational analysis could not isolate any effect of the inundation on the convection.

Citation: Prigent, C., N. Rochetin, F. Aires, E. Defer, J.-Y. Grandpeix, C. Jimenez, and F. Papa (2011), Impact of the inundation occurrence on the deep convection at continental scale from satellite observations and modeling experiments, *J. Geophys. Res.*, *116*, D24118, doi:10.1029/2011JD016311.

1. Introduction

[2] Despite their limited extent at a global scale (roughly 5% of the ice-free continental surfaces), wetlands play a key role in the global biogeochemical and hydrological cycles [*Alsdorf et al.*, 2007]. Their impact on the greenhouse effect has triggered significant interest lately, with 20 to 40% of the atmospheric methane emitted by wetlands, with strong interannual variability [*Bousquet et al.*, 2006; *Bloom et al.*, 2010; *Ringeval et al.*, 2010]. Their role on the local weather and climate also started to attract some attention. *Taylor* [2010] examined the feedbacks of the Niger Inland Delta on the precipitation and concluded that the presence of wetland increases rainfall in the region. The importance of the interaction between the land surface properties and the atmospheric convective activities is now well recognized [e.g., *Pielke*, 1984; *Georgescu et al.*, 2003; *Betts*, 2009], but its complexity is still not fully understood, and as a consequence not well represented in mesoscale models nor in climate models. Partitioning of the energy incident at the Earth's interface clearly depends upon the water availability at the surface, with strong impact on the convective activity, but the complex mechanisms at play are not all understood. On one hand, increasing water availability at the surface over a large area (e.g., hundreds of km) tends to increase evaporation and thus boundary layer moisture, which favors moist convection. This process is in agreement with *Rabin et al.* [1990] who observed that convective precipitation frequency is higher over wet areas. On the other hand, over drier surfaces the amplitude of the temperature diurnal cycle is larger and the boundary layer is deeper, which yields stronger updrafts. Simultaneously, the larger evaporation of precipitation induces stronger density currents, which also

[1]Laboratoire d'Etudes du Rayonnement et de la Matière en Astrophysique, CNRS, Observatoire de Paris, Paris, France.
[2]Laboratoire de Météorologie Dynamique/IPSL/CNRS, Université de Paris VI, Paris, France.
[3]Estellus, Paris, France.
[4]Also at Laboratoire d'Etude du Rayonnement et de la Matiére en Astrophysique, CNRS, Observatoire de Paris, Paris, France.
[5]Labaoratoire d'Etude du Rayonnement de la Matiére en Astrophysique, Observatoire de Paris, Paris, France.
[6]Laboratoire d'Etudes en Géophysique et Océanographie Spatiales, IRD, Toulouse, France.

Copyright 2011 by the American Geophysical Union.
0148-0227/11/2011JD016311

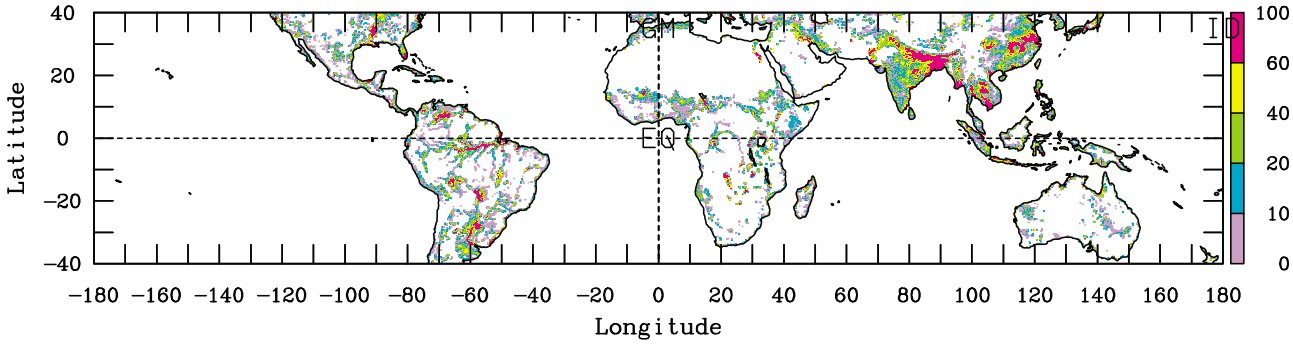

Figure 1. Mean inundation at yearly maximum over 1998–2000 in percentage of the 0.25° × 0.25° equal area grid.

favors stronger updrafts. This study analyzes which process dominates the occurrence of very deep convection at the continental scale. The complicated temporal dynamics of the wetland surface conditions, potentially very dry to completely inundated during the annual cycle, makes the analysis of the surface/atmosphere interaction even harder.

[3] In this study we examine the impact of the surface conditions of large wetlands on the convective activity at continental scales, first from an observational point of view. A consistent database of wetland extent and dynamics is now available, for the globe, with temporal and spatial resolutions compatible with seasonal and interannual analyses [*Prigent et al.*, 2007; *Papa et al.*, 2010]. The main challenge is to disentangle the direct impact of the convection on the wetland through precipitation, from the impact of the wetland on the convection itself. For local analysis such as presented by *Taylor* [2010], knowledge of the local atmospheric situation and transport makes it possible to separate these two aspects, but at continental scale, it is more difficult. In this study, a careful observational analysis of the seasonal and diurnal cycles of the convection, with respect to the inundation cycle will be conducted at continental scale to help isolate the effect of the wetland surface conditions on the convection. It will cover the tropical region between 40°S and 40°N, for 3 years. Second, modeling experiments will be carried out to test the conclusions of the observational analysis.

[4] Three major sources of satellite-derived databases are analyzed, between 1998 and 2000, over the tropics: a multisatellite wetland extent and dynamics data set, a deep convective activity index derived from passive microwave satellite measurements at 85 GHz, and precipitation estimates from the Global Precipitation Climatology Project (GPCP). The data sets are presented in section 2 and analyzed in section 3. Section 4 describes the modeling experiment and discusses the results. Conclusions are presented in section 5.

2. The Observational Data Sets

2.1. Satellite-Derived Surface Water Extent

[5] A method has been developed to detect inundation and to quantify their seasonal and spatial dynamics at global scale, using a suite of complementary satellite observations including passive and active microwaves, along with visible and infrared measurements [*Prigent et al.*, 2001a, 2007; *Papa et al.*, 2010]. Monthly mean wetland extent for 12 years (1993–2004) for the globe at a 0.25° × 0.25° spatial resolution at the equator (equal area grid) is now available. It has been used in several studies, for hydrological model evaluation [e.g., *Decharme et al.*, 2008] or for methane related issues [e.g., *Bousquet et al.*, 2006; *Ringeval et al.*, 2010]. Figure 1 presents the annual maximum fractional inundation averaged over 1998–2000 over the tropical region. The multisatellite inundation results show very realistic distributions, with major inundated wetlands well captured, for all types of environments. For instance, the region of high-inundation extent around the Himalaya corresponds to the melting of the snow at the end of the winter. These estimates, and their seasonal to interannual variations have been carefully evaluated by comparison with river height (from *in situ* measurements and from satellite altimeter estimates), with *in situ* river discharge, and with high-resolution maps of open water in the Amazon basin derived from Synthetic Aperture Radar (SAR) estimates of the water extent when available [*Prigent et al.*, 2007; *Papa et al.*, 2010]. Note that the data set of satellite-derived surface water extent is independent of the observations used to analyze the deep convective activity: the inundation detection and quantification are based on passive microwave observations at 19 and 37 GHz from the Special Sensor Microwave/Imager (SSM/I), whereas the convection is detected from passive microwave measurements at 85 GHz from another instrument onboard a different satellite (see section 2.2.)

2.2. Deep Convective Activity as Described From Microwave Scattering Over Ice Clouds at 85 GHz

[6] Depending on the wavelength and on the cloud properties, the microwave radiation observed from a satellite can be affected by emission, absorption, or scattering. Emission/absorption by liquid water particles causes the brightness temperature to increase, especially over a radiatively cold background like the ocean. In contrast, scattering by the larger hydrometeors generally reduces the measured brightness temperature. Ice particles absorb much less than liquid particles so the scattering effect dominates when they are present in the upper portions of the convective clouds. This effect increases with the ratio between the particle size and the wavelength of observations: the higher the frequency, the stronger the scattering signal. Compared to

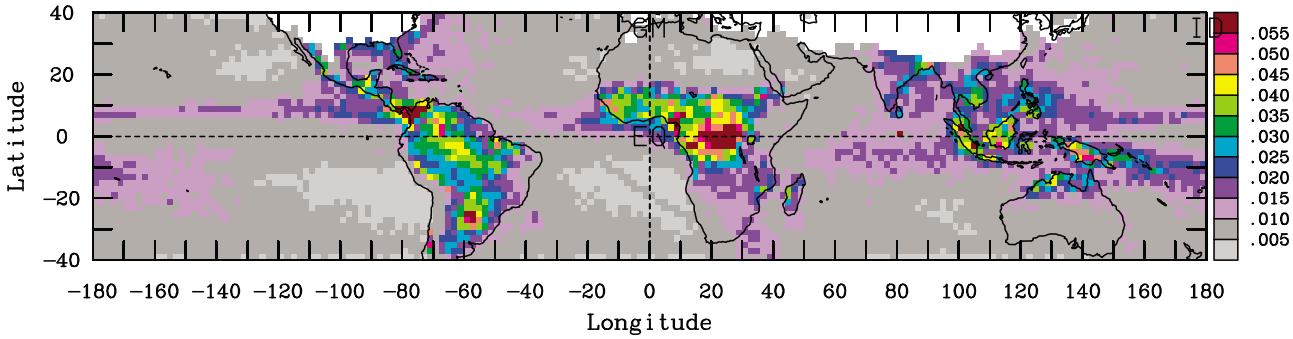

Figure 2. Global map of convective activity, averaged over 3 years, as given by the percentage of observations with Tb85V lower than 175 K over the total number of observations per 2° × 2° pixel. Potentially snow covered pixels have been filtered out using NSIDC products.

infrared observations, microwave signals penetrate deeper in the cloud structure and show more dynamics in the analysis of the convective activity than their infrared counterpart that tends to saturate.

[7] The Tropical Rainfall Measuring Mission (TRMM) Microwave Instrument (TMI) [*Kummerow et al.*, 1998] provides observations from 10 to 85 GHz. The TRMM platform is on a low equatorial orbit and observations of the intertropical zone (±40°) cover the full diurnal cycle. Several studies aimed at characterizing the convective activity from passive microwave observations around 85 GHz [*Nesbitt et al.*, 2000; *Nesbitt and Zipser*, 2003; *Prigent et al.*, 2001b, 2005; *Cecil et al.*, 2005; *Liu and Zipser*, 2005]. Convection is directly characterized by the 85 GHz brightness temperatures at vertical polarization (Tb85V): the lower the temperature, the larger the scattering by ice large particles, and the deeper the convection. H polarization would provide similar signatures, but is more likely to be contaminated by surface effects, over snow or ice covered regions. Polarized scattering signatures are observed over convective clouds [*Prigent et al.*, 2001b, 2005], but this is a second-order effect that will not be studied here. Several Tb85V thresholds have been tested in this study to detect scattering and a threshold at 175 K is selected, corresponding to very deep convection. This low threshold limits potential confusion with scattering from surfaces such as snow and dry sands. In order to have a statistically representative data set of deep convective events covering the full diurnal cycle, 3 full years of data are analyzed (1998–2000). Note that only microwave frequencies up to 37 GHz are used in the wetland detection and quantification processing: these low frequencies are not or very little sensitive to scattering by the cloud ice and, in addition, cloud contaminated pixels are disregarded in the wetland processing [*Prigent et al.*, 2007], thus avoiding any spurious relationship between the wetland estimates and the convection analysis.

[8] Figure 2 shows global maps of convective activity, averaged over 3 years, as given by the percentage of observations with Tb85V lower than 175 K over the total number of observations per 2° × 2° pixel. Potentially snow covered pixels have been filtered out from this map, using National Snow and Ice Data Center (NSIDC) products, in order to avoid any ambiguities between scattering by cloud ice and by snow on the ground. As expected, deep convective activity is present mostly over land. It has been verified that similar structure of the convective activity is observed with infrared/visible observations in the International Satellite Cloud Climatology Project (ISCCP) database [*Rossow and Schiffer*, 1999].

2.3 Precipitation Estimate From GPCP

[9] The monthly mean GPCP product quantifies the distribution of precipitation around the globe over many years, from merged rain gauge measurements and infrared and microwave satellite data [*Adler et al.*, 2003]. We use for 1998–2000 the monthly mean GPCP products (Version 2).

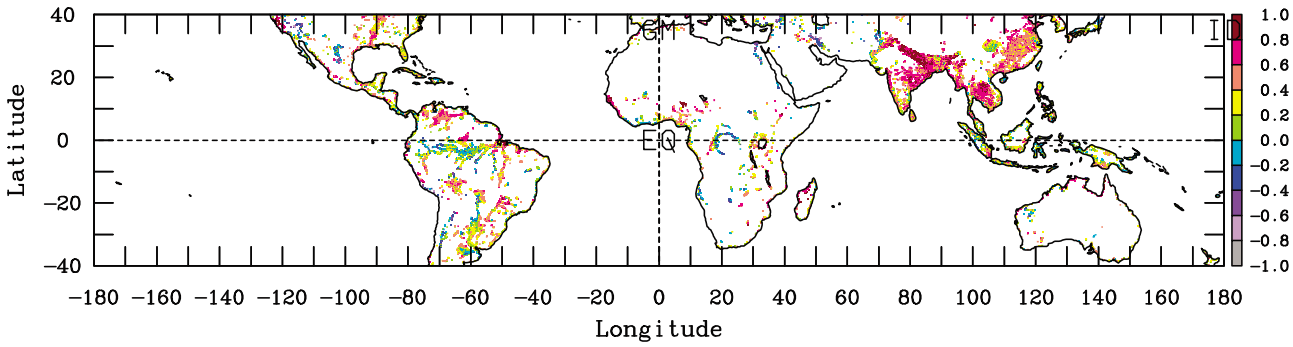

Figure 3. Correlation between the monthly wetland extent and precipitation (GPCP) gridded to the 0.25° × 0.25° at the equator equal area grid over 1998–2000.

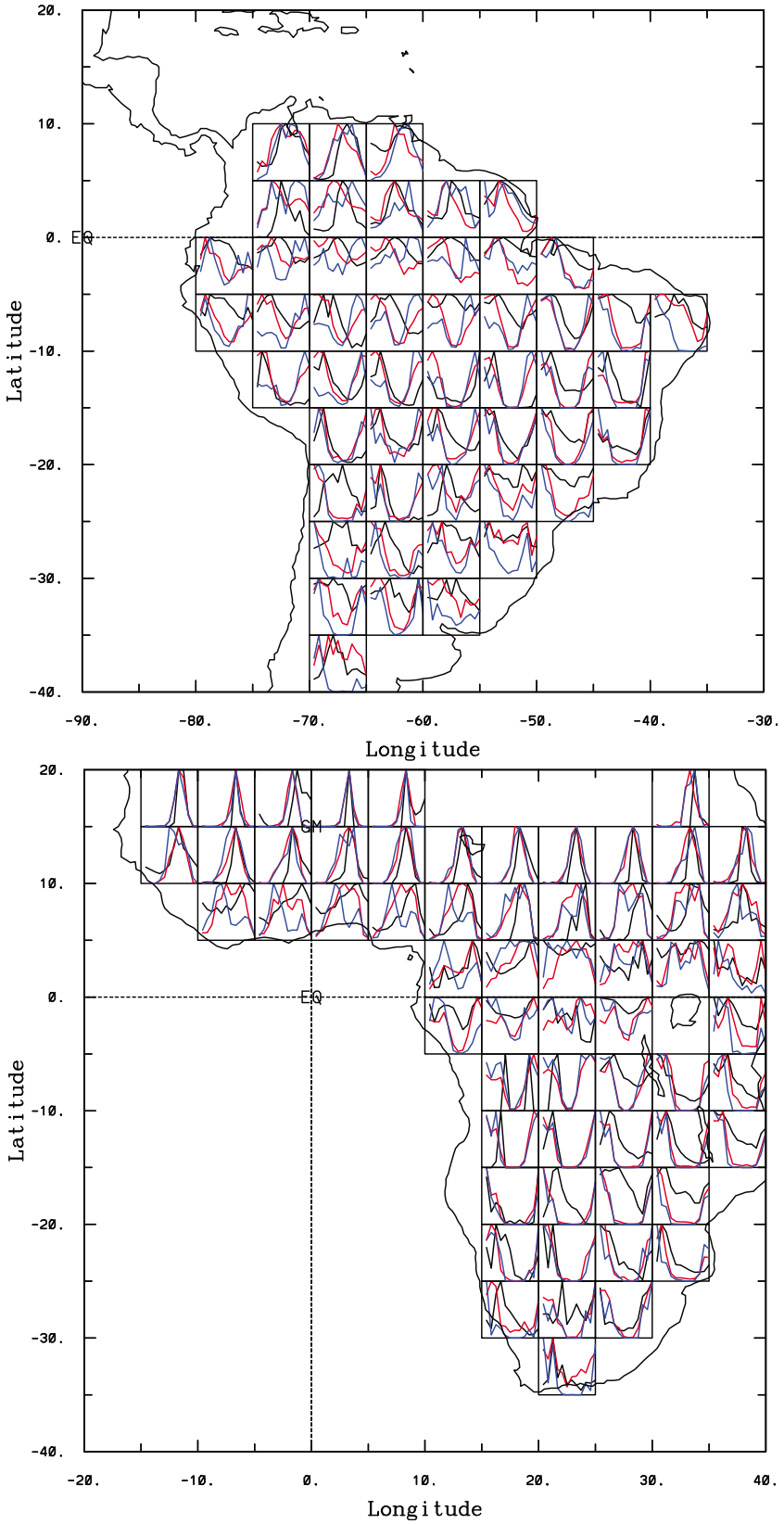

Figure 4. Comparison of the seasonal cycles of different variables, from January to December, averaged over 1998–2000. The inundation (multisatellite retrieval) is in black, the precipitation (GPCP) is in red, and the deep convection (Tb 85 GHz below 175 K) is in blue. The data are gridded on 5° × 5° (top) in South America and (bottom) in Africa. Each seasonal cycle is normalized to 1. See Figure 5 for a zoom over two regions in South America and in Africa.

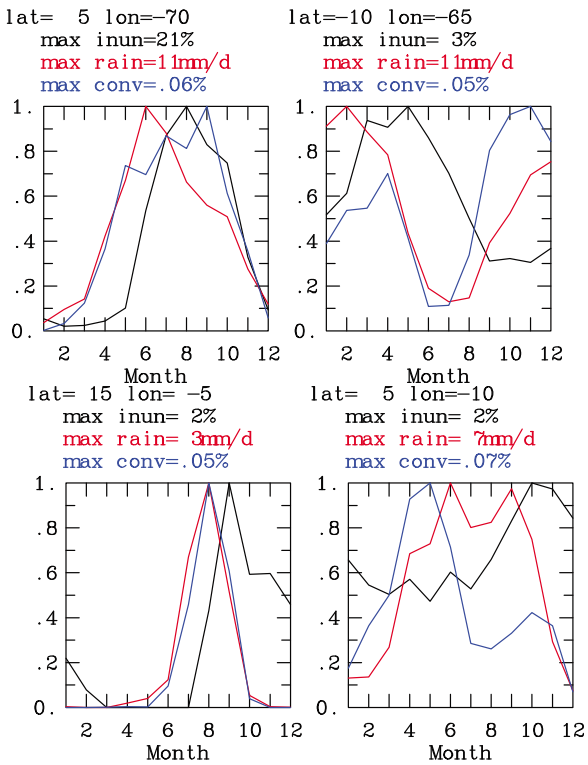

Figure 5. Same as Figure 4 but zoomed on two regions (5° × 5°) with contrasted behaviors in South America over (top left) the Orinoco basin and over (top right) the Amazon basin and in Africa over (bottom left) the Niger basin and over (bottom right) the Congo basin. The southwest corner of each grid is indicated as well as the maximum value of each curve.

The estimates uncertainties in GPCP products over land range from 10 to 30%.

3. Observational Analysis of the Impact of Inundated Wetlands on the Convection

[10] Different processes can generate inundation: it can be related to local precipitation as well as to rainfall or snowmelt upstream. In regions where convective precipitation generates local inundations, such as in monsoon regimes over the Indian Subcontinent or over South East Asia, the feedback of the wetland on the convection is difficult to separate from the direct effect of the convective precipitation on the inundation. This study is an attempt to evidence the effect of the inundation on the convection, by carefully analyzing the time variation of the convection with respect to the inundation dynamics, at seasonal and diurnal scales.

3.1 The Link Between the Seasonal Cycle of the Inundation, the Deep Convection, and the Precipitation

[11] The linear correlation between the monthly mean inundated surfaces and the GPCP precipitation estimates have been calculated, on a global basis, for 1998–2000. The results are mapped in Figure 3. The linear correlation is positive and large (above 0.6) in regions with strong precipitation seasonal cycles and rather low vegetation density. For instance, in India where a monsoon regime dominates the precipitation cycle, the inundation extent is strongly correlated with precipitation. In other regions, the precipitation and inundation cycles are lagged. The correlation is generally higher in the surrounding part of the basin and decreases around the main stream, such as around the Pantanal, with the correlation increasing with the distance from the Paraguay River. Around the main stem of the Amazon River, the correlation is also relatively low and increases along the tributaries. See *Prigent et al.* [2007] and *Papa et al.* [2006] for more details, especially in South America. The correlation between the deep convection and the inundation shows similar patterns as the correlation between the precipitation and the inundation (not presented here).

[12] In order to examine the relationship between these variables more closely, Figure 4 represents the seasonal cycle of the deep convective activity (as described by the percentage of observations with Tb85V lower than 175 K in blue), compared to the seasonal cycle of the inundation (in black), and to the seasonal cycle of the GPCP precipitation (in red), for South America and a large part of Africa. The data are averaged over 5° × 5° squares, for the 3 years. The 5° × 5° presentation is chosen here to provide more readable figures (other space averagings have been tested with similar conclusions). For each 5° × 5° grid cell, each seasonal cycle is normalized to 1. Figure 5 zooms on two specific regions with contrasted behaviors in South America (Figure 5, top) and in Africa (Figure 5, bottom). The latitude and the longitude of the southwest corner of the region are indicated, as well as the maximum of each curve.

[13] In regions of significant correlations between the precipitation and the inundation cycle (e.g., north of 5°N or east of −50°W in South America or north of 10° in Africa), the convective activity also follows similar seasonal cycles. In these regions, there are two clearly distinct seasons, a wet and a dry one, with very limited rainfall during the dry season. Zooms at 5°N–70°W in South America in the Orinoco basin and at 15°N–5°W in the Niger basin in Africa show that the seasonal cycles in these regions are similar, with limited time lags between the variables (Figure 5, left). On the contrary, in regions where the seasonal cycles of precipitation and inundation are not correlated, the seasonal cycle of the deep convection is phased neither with the precipitation nor with the inundation. This is the case in the Amazon basin south of the equator, as well as in southwest Africa. Two specific examples are presented in Figure 5 (right). The maximum of the convection tends to occur when the inundation is close to its minimum. In these regions, variations of the inundated surfaces are less sensitive to the local, high-frequency forcing, but act as a long-term forcing for convection. The full ±40° latitude band has been examined. In South Asia for instance, the monsoon regime clearly dominates, with similar seasonality of the inundation, the precipitation, and the convective activity. The seasonal cycle of the convective activity remains analogous when using a microwave T85V threshold at 200 K instead of 175 K. Results were also examined at 2° × 2° horizontal resolution: similar conclusion could be drawn.

[14] A provisional conclusion is that two main regimes are identified. In regions where inundation is generated by local precipitation, the soil wetness is a direct response to the local atmospheric forcing, the convective activity is directly related to the precipitation and the feedback of the

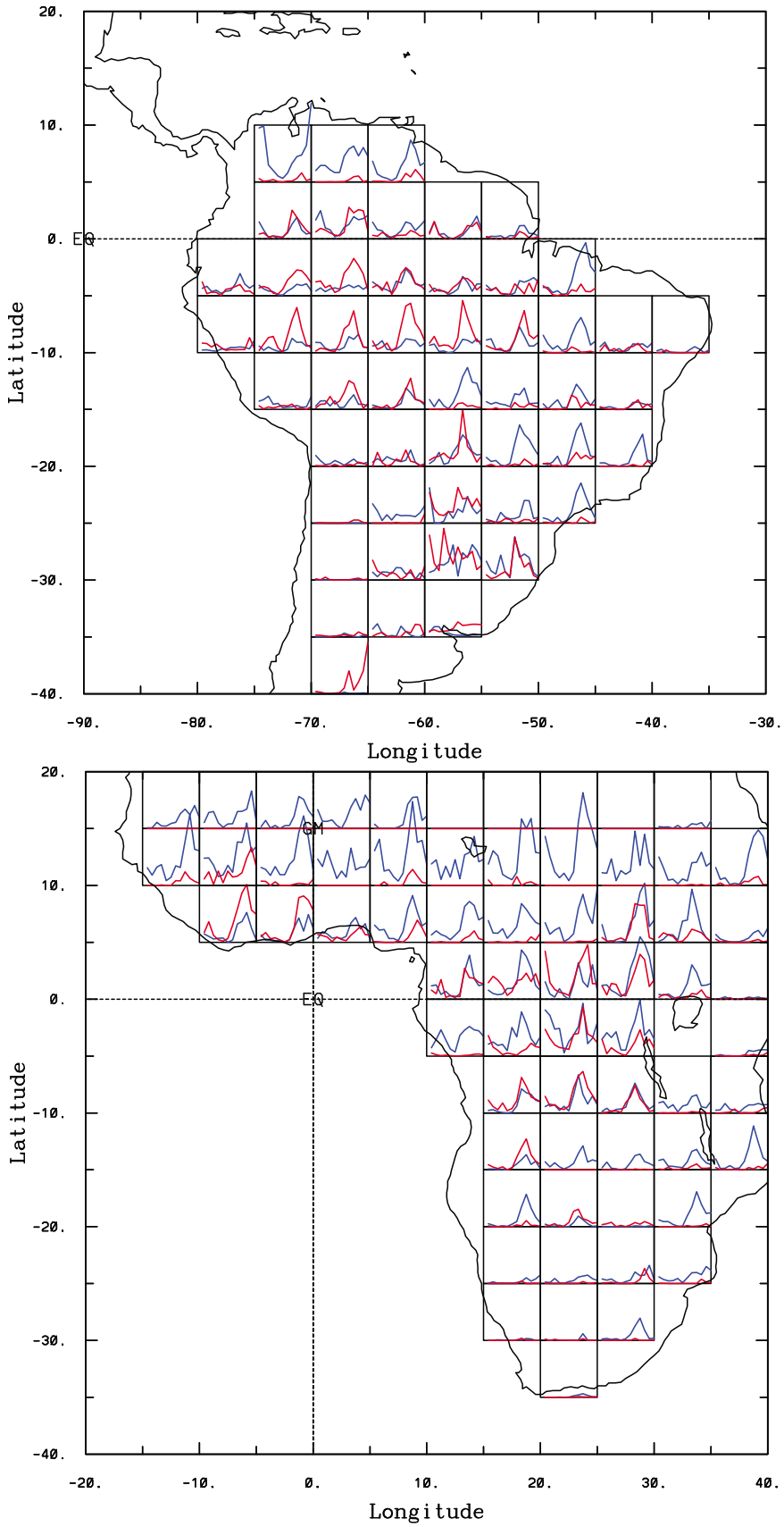
20.
10.
0. EQ
-10.
-20.
-30.
-40.
Latitude
-90.
-80.
-70.
-60.
-50.
-40.
-30.
Longitude
20.
GM
10.
0.
EQ
-10.
-20.
-30.
-40.
Latitude
-20.
-10.
0.
10.
20.
30.
40.
Longitude

Figure 6

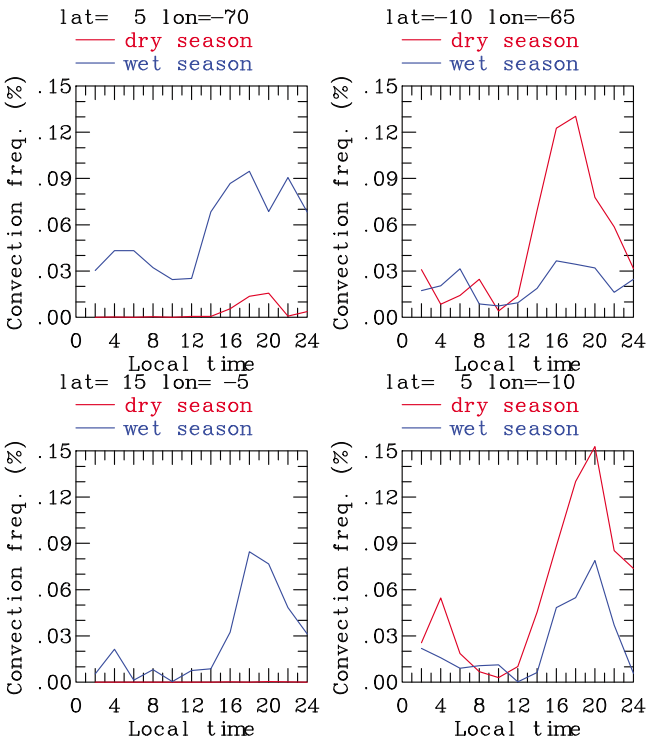

Figure 7. Same as Figure 6 but zoomed on two regions (5° × 5°) with contrasted behaviors in South America over (top left) the Orinoco basin and over (top right) the Amazon basin and in Africa over (bottom left) the Niger basin and over (bottom right) the Congo basin. The southwest corner of each grid is indicated.

inundation on the convective activity cannot be evidenced with our analysis. These regions also correspond to pronounced wet and dry seasons, typical of semiarid zones. In regions where inundation is due to rain upstream, the maximum of the convective activity tends to occur during the minimum of the inundation. The coincidence of these two seasonal phenomena do not imply that a causal relationship exists between them. However, a tentative explanation is that drier surfaces favor the generation of updrafts that feed the convection. If this is true, the diurnal cycle of convection should vary from the dry to the wet season, with a marked increase of the convective activity in the afternoon for drier conditions, due to solar heating of the drier surface.

3.2 Diurnal Cycle of the Convection in Inundated Regions

[15] One way to test our hypothesis is thus to analyze the diurnal cycle of the convection. Figure 6 represents the diurnal cycle of the deep convective activity (as described by the percentage of observations with Tb85V lower than 175 K), for the seasons that correspond to the minimum (in red) and to the maximum (in blue) of the inundation, over South America (Figure 6, top) and over a large part of Africa (Figure 6, bottom). The dry and wet periods are the mean of the 3 months that correspond to the minimum and maximum of the inundation in the year. The data are averaged over 5° × 5° squares, for the 3 years. Similar to Figure 5, Figure 7 zooms on the two specific regions with contrasted behaviors already discussed in section 3.1.

[16] Here again, two distinct regimes appear that seem to coincide in space with the two regimes previously described in terms of seasonal cycles. In regions where the convective activity is stronger during the minimum of inundation, the amplitude of the diurnal cycle of the convection clearly peaks in the afternoon, whereas during the maximum of the inundation it is rather limited. The averaged result over the 3 studied years is shown in Figures 6 and 7, but we checked that these temporal patterns are reproduced each single year. This supports our hypothesis, namely that the drier surface, under solar heating, feeds the convective activity. In regions where the inundation, the precipitation, and the convection are correlated, there is very limited convection during the dry period and there is a marked diurnal cycle of the convection during the wet season, as expected.

4. Model Analysis of the Sensitivity of the Deep Convection to Inundation

[17] In this section, the physical interaction between inundation and deep convection is analyzed, using the Single Column Model (SCM) from the Laboratoire de Météorologie Dynamique (LMD)'s Global Climate Model (GCM) (LMDZ4). The SCM will be used in an ideal case of radiative convective equilibrium (RCE) to better understand the role of soil wetness on the convection in regions where large-scale moisture transport is limited.

4.1 Description of the Single Column Model

[18] The SCM from the LMD GCM (LMDZ4) is used to perform climate change simulations for the 4th IPCC assessment report [*Hourdin et al.*, 2006].

[19] Emanuel's cumulus parameterization [*Emanuel*, 1991] is adopted for moist convection. For convective anvils, the Emanuel scheme computes a total cloud water content. Note that this convective scheme does not contain any ice parameterization. It is coupled to a statistical cloud representation based on the computation of a cloud fraction using a lognormal probability density function [*Bony and Emanuel*, 2001].

[20] Since the last report by the *Intergovernmental Panel on Climate Change* [2007], main improvements in the LMD SCM concern the computation of deep convection triggering and closure. The convection scheme is coupled to a parameterization of shallow moist convection induced by

Figure 6. Comparison of the diurnal cycles of the deep convection (Tb 85 GHz below 175 K) for 5° × 5° regions (top) in South America and (bottom) in Africa during wet and dry seasons for 1998–2000. Data are binned over 1 h periods. The diurnal cycle of the convection during the drier period of the year (mean of the 3 months that correspond to the minimum of the inundation) is in red, and the diurnal cycle during the wetter period of the year (mean of the 3 months that correspond to the maximum of the inundation) is in blue. The vertical scale goes from 0% to 0.15% of deep convective activity. See Figure 7 for a zoom over two regions in South America and in Africa.

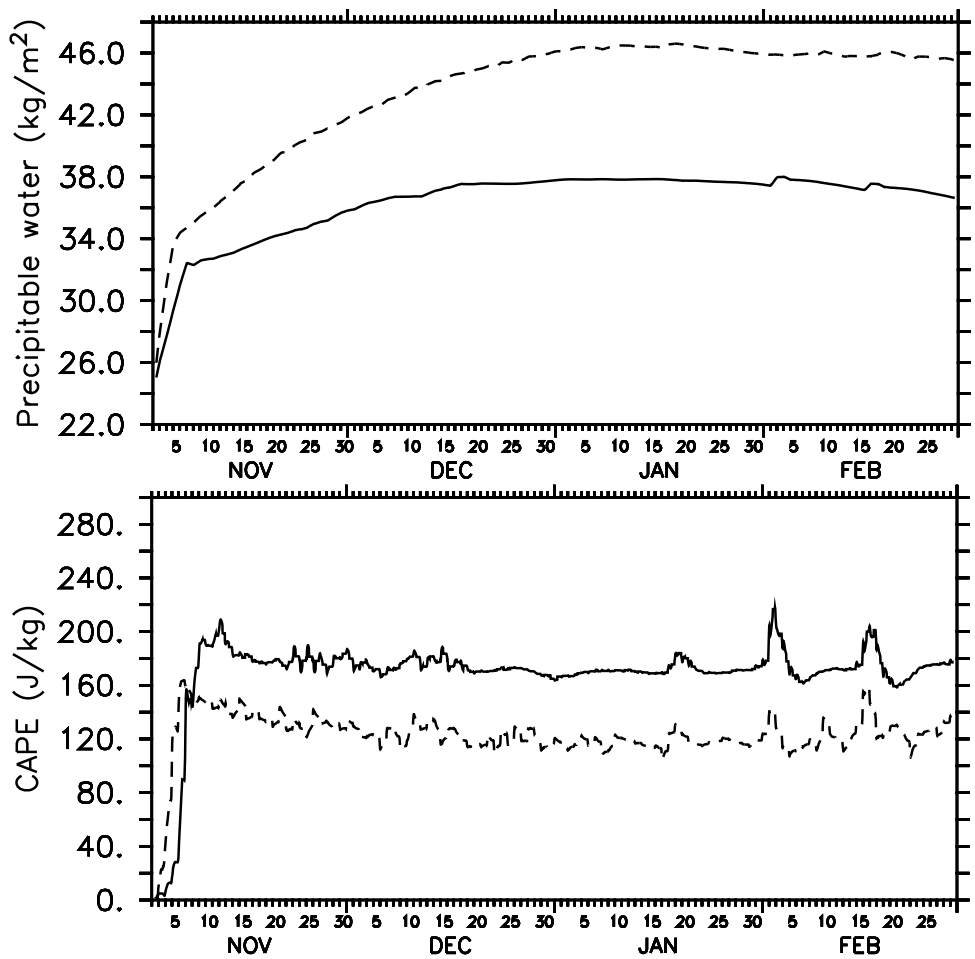

Figure 8. Time series of (top) daily mean precipitable water and (bottom) convective available potential energy (CAPE) for the dry (β = 0.25, solid lines) and wet (β = 0.7, dashed lines) cases.

thermal plumes [*Rio and Hourdin*, 2008], and to a parameterization of wakes (cold pools) fed by unsaturated downdrafts [*Grandpeix and Lafore*, 2010a]. These parameterizations provide the deep convection scheme with an available lifting energy related to the convection triggering computation and an available lifting power related to the convection closure computation [*Grandpeix and Lafore*, 2010b]. It improves the diurnal cycle of precipitation over lands [*Rio et al.*, 2009].

[21] Turbulent fluxes in the boundary layer are computed with the diffusive scheme from *Mellor and Yamada* [1974]. A soil thermal diffusion and groundwater storage model is used, and surface fluxes are calculated with the Monin-Obukhov similarity method.

4.2 Methodology

[22] The tropics are often assumed to experience a balanced state of RCE [*Tompkins and Craig*, 1999; *Tompkins*, 2001] with the temperature profile constrained by the moist adiabatic profile [*Larson and Hartmann*, 2003]. The RCE hypothesis corresponds to a perfect balance between surface heat fluxes and radiative cooling regarding a long enough period. Indeed the time scale of interest is largely superior to the lifetime of an individual convective system. This hypothesis assumes that the tropics can be described as a closed Hadley cell that does not interact with the extratropics.

[23] In oceanic RCE cases, fixed sea surface temperature (SST), albedo and surface wind are prescribed; the insolation is constant and the solar zenith angle is set to zero, so that the diurnal cycle is removed. This is consistent with the quasi absence of diurnal fluctuations of SST and radiative budget profile observed over tropical oceans.

[24] We propose to use our SCM in a continental RCE case, i.e., in a case where the diurnal cycle of surface temperature plays an important role which makes it necessary to use a solar forcing with diurnal cycle and to fix the soil temperature at a depth large enough so that the full surface temperature diurnal cycle may be simulated. We use a simple, thermal diffusion only, soil model and we nudge the temperature at ~10 cm toward an arbitrary value of 295 K.

[25] In this experiment, two contrasted situations are compared, one with a dry soil, the other one with a wet soil. The only difference between the two runs is the prescribed evapotranspiration coefficient β that corresponds to the ratio of the effective evaporation over the potential evaporation. β is generally related to soil wetness (over ocean, β = 1); in the case of inundated areas, it is linked to the area percentage of inundated surfaces, as defined in section 3. Two β conditions are presented (many more were tested): (1) β = 0.25 for rather dry surface with occasional puddles and (2) β = 0.70 for very saturated soil including wetlands.

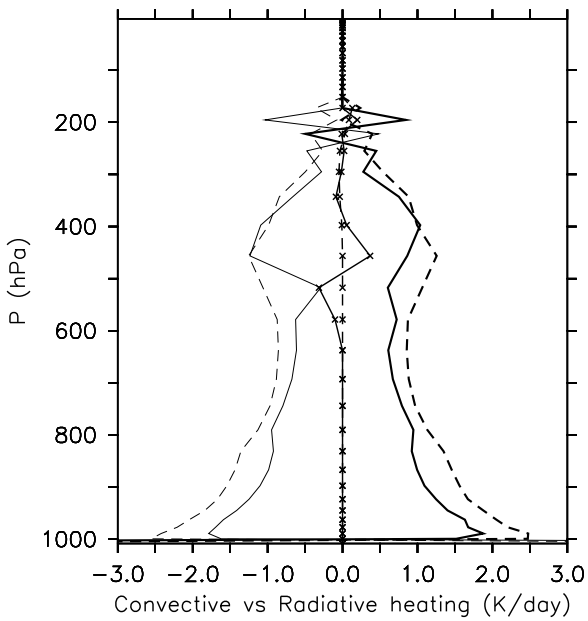

Figure 9. Averaged radiative heating (thin lines), convective heating (thick lines), and large-scale condensation heating (crosses) profiles for the dry (solid lines) and wet (dashed lines) cases at equilibrium.

[26] A run of 120 days with a 2 min time step is performed for each case (dry and wet surfaces) with a diurnal cycle forcing and a diffusive surface. The initial solar forcing corresponds to 2 November, midnight local time, and the surface initial temperature is set to 300 K.

4.3 Results and Discussion

[27] After ~60 day period, the time series of precipitable water (PRW) and convective available potential energy (CAPE) exhibit a permanent regime for both dry and wet cases, indicating that equilibrium has been reached in terms of water and energy cycles (Figure 8). Note that the time series of instantaneous CAPE and PRW exhibits diurnal oscillations around their mean value (not shown). Indeed, the continental RCE oscillates around its equilibrium state, while the oceanic RCE is stationary. The steady state for PRW denotes the balance between evaporation and precipitation, this value corresponds to the mean water vapor amount stored by the convecting atmosphere at equilibrium. In the wet case, the column integrated water vapor is more important than in the dry case because of an enhanced surface evaporation. The CAPE quantifies the average departure from the moist adiabatic profile at equilibrium, i.e., the overall energy stored in the high atmosphere. This constant CAPE highlights the energy balance between convective heating and radiative cooling. The lower CAPE observed in the wet case indicates that more energy is consumed by convection and less energy remains in the atmosphere.

[28] Figure 9 shows the averaged heating profiles for January and February. Under wet conditions, the radiative cooling strictly balances the convective heating, with a value close to zero all along the vertical. Under dry conditions, deep convection does not perfectly compensate radiative cooling all along the atmospheric column, so that large-scale condensation and evaporation occur between 600 hPa and 400 hPa. Over wet surfaces, the Bowen ratio (sensible heat flux over the latent heat flux) is lower and the overlying atmosphere contains more water vapor (Figure 8, top). The presence of more water vapor in the midtroposphere not only improves the precipitation efficiency [*Tompkins*, 2001; *Anthes*, 1977; *Raymond*, 1995], it also increases the optical thickness of the atmosphere and, as a consequence, the clear-sky radiative cooling resulting in a more intense compensating convective heating. As a result, the convective heat engine is more efficient [*Rennó*, 1997; *Rennó et al.*, 1994a, 1994b]. Note that the cloud feedback on radiative cooling is also important, especially in the dry case (not shown). In the following, only the equilibrium period will be considered; the first 2 months are representative of the time scale of adjustment and will not be analyzed.

[29] Time series of surface temperatures are extracted at equilibrium (Figure 10). The amplitude of the surface temperature diurnal cycle is larger under dry conditions than under wet conditions, as expected: the drier the surface, the higher the Bowen ratio (i.e., the incoming solar energy is preferentially released by sensible than by latent heat) and the surface temperature during daytime. In addition, as the minimum values are similar in both cases, the mean surface temperature at equilibrium is slightly higher in the dry case, with potential impact on the convection depth.

[30] The TRMM satellite observations previously analyzed provide information on the deep convective activity. For comparison with the satellite data, the relevant model output is the convective cloud ice water content q_{ice} (kg/kg). It is derived from the computation of the convective cloud liquid water content q_{liq} (kg/kg) inside the mixed updrafts. In *Emanuel*'s [1991] convection scheme, those saturated updrafts result from the mixing between undiluted adiabatic ascent and the entrained environmental air. An estimate of q_{ice} is computed from the q_{liq} and the environment temperature T. It is assumed that the ice conversion in the mixed updrafts starts at $T_{\max}$ = °C and finishes at $T_{\min}$ = −15°C, i.e., no liquid water can be found below the −15°C isotherm. Between 0°C and −15°C, a linear conversion rate is calculated $q_{ice} = q_{liq} * (\frac{T_{\max}-T}{T_{\max}-T_{\min}})$.

[31] Time series of the q_{ice} are displayed in Figure 11, averaged over the equilibrium period, for both dry and wet

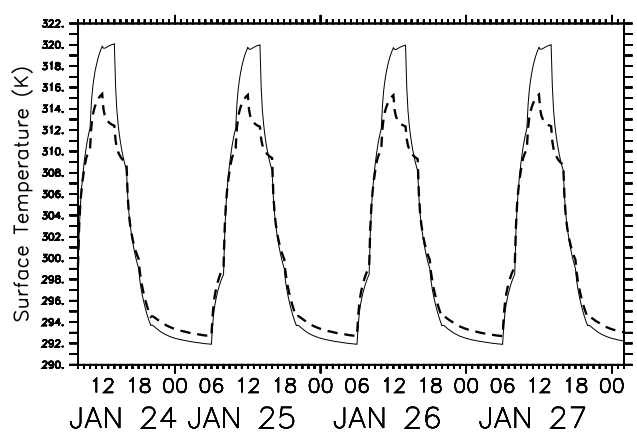

Figure 10. Time series of the surface temperature for the 24–28 January period for the dry (thin solid) and the wet (thick dashed) cases. The time axis is solar local time.

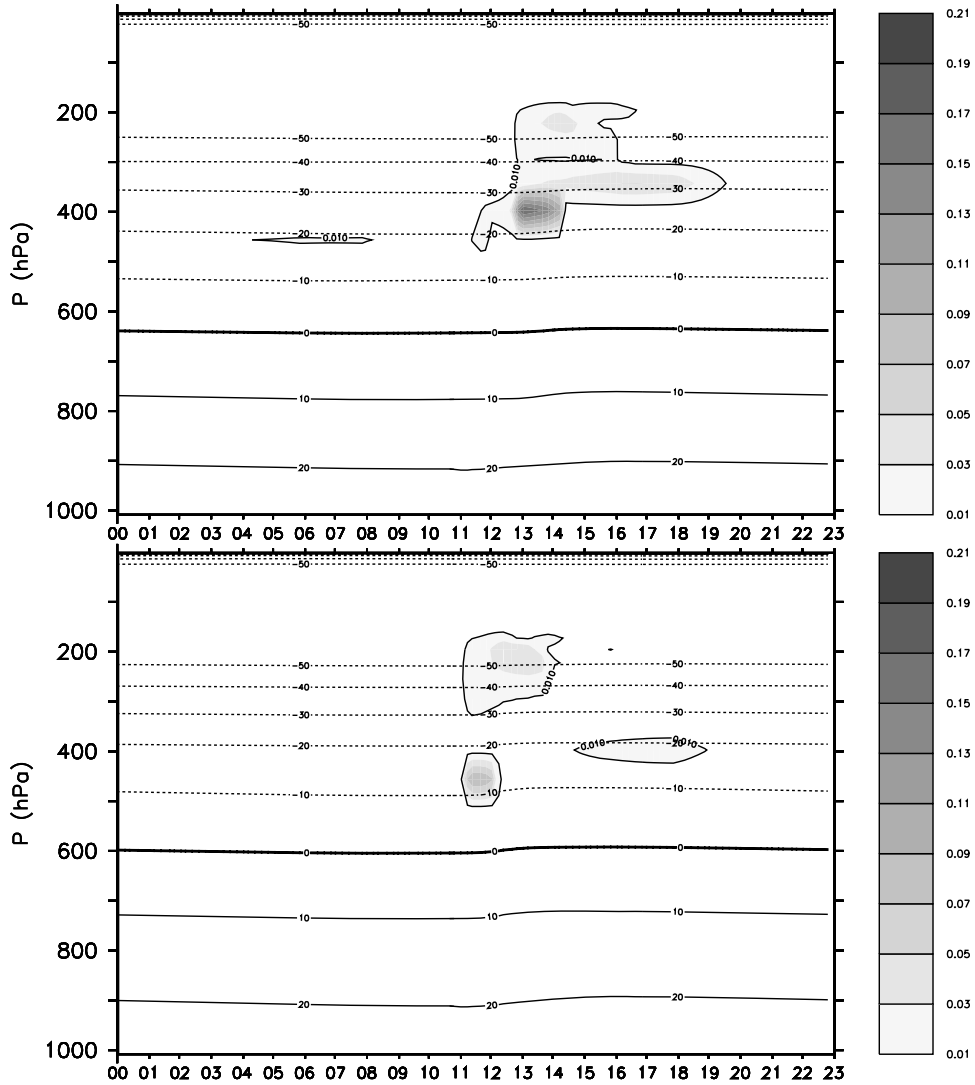

Figure 11. Diurnal cycle of the convective cloud ice content (shaded) (g/kg) and temperature of the environment (contoured) (°C) averaged over the equilibrium period for the (top) dry and the (bottom) wet cases. The additional contour line is the 0.01 g/kg isoline for q_{ice}.

cases. Under drier conditions, larger ice quantities are created, in agreement with the TRMM satellite-derived observations. The ice concentrations are much larger and located higher in the atmosphere. Indeed the maximum concentration q_{ice} (between 13 h and 14 h for the dry case and between 11 h and 12 h for the wet case) is two times more important in the dry case and located between the −20°C and −30°C isotherms while it is located between the −10°C and −20°C for the wet case. The model shows that over drier surfaces, deep convection tends to produce condensed phases at higher altitudes, i.e., in a colder environment that likely generates larger ice concentrations. This is true throughout the convective activity, even during the decaying phase. This agrees with the TRMM satellite observations of the deep convection and supports the tentative explanation we suggested.

[32] It appears that the key parameter is the surface temperature and similar conclusions have been drawn over ocean. *Tompkins and Craig* [1999] and *Larsonn and Hartmann* [2003] used a CRM over a uniform ocean and analyzed the sensitivity of convection to sea surface temperature under radiative-convective equilibrium (no large-scale flow). They found that when surface temperature increases, convection produces more ice and other condensed phases at higher levels. *Tompkins and Craig* [1999] explain that over a warmer surface a parcel undergoing ascent through deep convective cloud experiences approximatively the same range of temperature but at higher altitudes (i.e., lower pressures), favoring saturation of water, and hence ice conversion. Moreover, if the isotherms are shifted upward inside the adiabatic ascent, the parcel experiences also a colder adjacent environmental air: this could also play a crucial role favoring at the same time production of ice by entrainment and important buoyancy forces that can sustain heavier hydrometeors and support their growth by riming [*Houze*, 2004].

[33] The time series of the vertically integrated q_{ice} is represented in Figure 12. The diurnal cycle of integrated q_{ice} is much stronger over dry areas than over wet regions. In the dry experiment, the maximum concentration of ice reaches 0.28 g/kg during the precipitating phase while it is

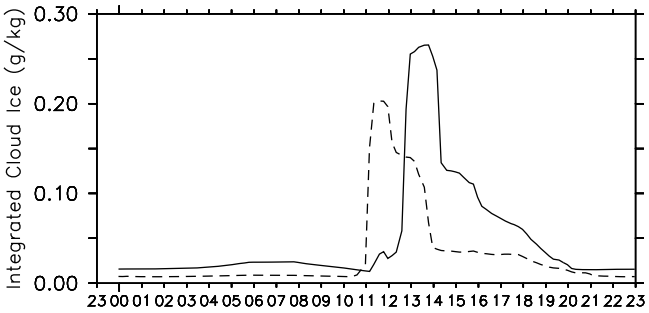

Figure 12. Diurnal cycle of vertically integrated convective cloud ice content (g/kg) averaged over the equilibrium period for the dry (solid lines) and the wet (dashed lines) cases.

only 0.2 g/kg for the wet run. This result agrees with the observations in Figure 7 and is compatible with our initial hypothesis; the daytime distribution of deep convection in terms of ice concentration is more peaked over dry areas. Figure 12 suggests also that the deep convection exhibits three phases under both dry and wet conditions. The first phase lasts ~1 h 30 min in the dry case and ~1 h in the wet case in which convection intensity is at its maximum and convective precipitations are increasing (not shown). The integrated q_{ice} reaches its maximum value and vertical extent (see Figure 11), with the convective towers reaching up to ~200 hPa (which is the typical detrainment altitude of convective cloud [see *Larson and Hartmann*, 2003]). The following stage is a 2 h long decreasing phase of convective activity characterized by a decrease in convective precipitations (not shown) and a rapid decrease in q_{ice}. At the end of this phase, there is no more convective precipitation (not shown). It is followed by a long dissipation phase (4 h in the dry case and 7 h in the wet case) of very light convection: there is still convective heating by condensation, but the induced precipitations are so low that they evaporate before reaching the surface (not shown). During this stage q_{ice} decreases very slowly.

[34] As a consequence, the model simulations tend to support the two main conclusions derived from the satellite observations. First, for drier surfaces, the altitude and concentration of ice hydrometeors inside the anvil increase, essentially due to the larger surface temperature. The convective cloud ice concentration peaks higher above the freezing level in the dry case, enhancing the production of high ice concentration throughout the convective life cycle. Second, the amplitude of the diurnal cycle of the deep convective activity in terms of ice concentration is larger under drier conditions.

5. Conclusion

[35] From the detailed analysis of seasonal and diurnal variations of satellite-derived information over the tropics (±40°), during 3 years, this study evidences the impact of the inundation occurrence on the deep convection, at continental scale. Although many other effects contribute to the seasonal and diurnal variations (e.g., large-scale circulation and weather regimes), two distinct regimes are observed. The first regime corresponds to regions where the inundation is not generated by local precipitation. There, it is shown that strong convection happens during the minimum of the inundation, with a large diurnal cycle of the convective activity with a maximum in the late afternoon. Simulations with a single-column model derived from LMDZ4 are in good agreement with these observations: calculations show that during the drier season, hydrometeors are present higher in altitude, increasing the likelihood of larger ice quantities aloft, and the diurnal cycle of the convective activity related to large ice quantities is larger.

[36] The second regime corresponds to region where the inundation is directly generated by local precipitation. There, our observational analysis could not isolate any effect of the inundation on the convection.

[37] **Acknowledgments.** We would like to thank Katia Laval and three anonymous reviewers for their careful reading of the manuscript and their interesting suggestions.

References

Adler, R. F., et al. (2003), The version 2 Global Precipitation Climatology Project (GPCP) monthly precipitation analysis (1979–present), *J. Hydrometeorol.*, *4*, 1147–1167.

Alsdorf, D. E., E. Rodriguez, and D. P. Lettenmaier (2007), Measuring surface water from space, *Rev. Geophys.*, *45*, RG2002, doi:10.1029/2006RG000197.

Anthes, R. A. (1977), A cumulus parameterization scheme utilizing a one-dimensional cloud model, *Mon. Weather Rev.*, *105*, 270–286.

Betts, A. K. (2009), Land-surface-atmosphere coupling in observations and models, *J. Adv. Model Syst.*, *1*, 4–18.

Bloom, A. A., P. I. Palmer, A. Fraser, D. S. Reay, and C. Frankenberg (2010), Large-scale controls of methanogenesis inferred from methane and gravity spaceborne data, *Science*, *327*, 322–325, doi:10.1126/science.1175176.

Bony, S., and K. A. Emanuel (2001), A parameterization of the cloudiness associated with cumulus convection; evaluation using TOGA COARE data, *J. Atmos. Sci.*, *58*, 3158–3183.

Bousquet, P., et al. (2006), The contribution of anthropogenic and natural sources to the variability of atmospheric methane, *Nature*, *443*, 439–443, doi:10.1038/nature05132.

Cecil, D. J., S. J. Goodman, D. J. Boccippio, E. J. Zipser, and S. W. Nesbitt (2005), Three years of TRMM precipitation features. Part 1: Radar, radiometric, and lightning characteristics, *Mon. Weather Rev.*, *133*, 543–566.

Decharme, B., H. Douville, C. Prigent, F. Papa, and F. Aires (2008), A new river flooding scheme for global climate applications: Off-line evaluation over South America, *J. Geophys. Res.*, *113*, D11110, doi:10.1029/2007JD009376.

Emanuel, K. A. (1991), A scheme for representing cumulus convection in large-scale models, *J. Atmos. Sci.*, *48*, 2313–2335.

Georgescu, M., C. P. Weaver, R. Avissar, R. L. Walko, and G. Miguez-Macho (2003), Sensitivity of model-simulated summertime precipitation over the Mississippi River basin to the spatial distribution of initial soil moisture, *J. Geophys. Res.*, *108*(D22),8855, doi:10.1029/2002JD003107.

Grandpeix, J.-Y., and J.-P. Lafore (2010a), A density current parameterization coupled with Emanuel's convection scheme. Part I: The models, *J. Atmos. Sci.*, *67*, 881–897.

Grandpeix, J.-Y., and J.-P. Lafore (2010b), A density current parameterization coupled with Emanuel's convection scheme. Part II: 1D simulations, *J. Atmos. Sci.*, *67*, 898–927.

Hourdin, F., et al. (2006), The LMDZ4 general circulation model: Climate performances and sensitivity to parameterized physics with emphasis on tropical convection, *Clim. Dyn.*, *27*, 787–813.

Houze, R. A., Jr. (2004), Mesoscale convective systems, *Rev. Geophys.*, *42*, RG4003, doi:10.1029/2004RG000150.

Intergovernmental Panel on Climate Change (2007), *Climate Change 2007: The Physical Science Basis, Working Group I Contribution to the Fourth Assessment Report of the IPCC*, edited by S. Solomon et al., Cambridge Univ. Press, Cambridge, U. K.

Kummerow, C., W. Barnes, T. Kozu, J. Shiue, and J. Simpson (1998), The Tropical Rainfall Measuring Mission (TRMM) sensor package, *J. Atmos. Oceanic Technol.*, *15*, 808–816.

Larson, K., and D. L. Hartmann (2003), Interaction among cloud, water vapor, radiation, and large-scale circulation in the tropical climate. Part

I: Sensitivity to uniform sea surface temperature changes, *J. Clim.*, *16*, 1425–1440.

Liu, C., and E. J. Zipser (2005), Global distribution of convection penetrating the tropical tropopause, *J. Geophys. Res.*, *110*, D23104, doi:10.1029/2005JD006063.

Mellor, G. L., and T. Yamada (1974), A hierarchy of turbulence closure models for planetary boundary layers, *J. Atmos. Sci.*, *31*, 1791–1806.

Nesbitt, S. W., and E. J. Zipser (2003), The diurnal cycle of rainfall and convective intensity according to three years of TRMM measurements, *J. Clim.*, *16*, 1456–1475.

Nesbitt, S. W., E. J. Zipser, and D. J. Cecil (2000), A census of precipitation feature in the tropics using TRMM: Radar, ice scattering, and ice observations, *J. Clim.*, *13*, 4087–4106.

Papa, F., C. Prigent, F. Durand, and W. B. Rossow (2006), Wetland dynamics using a suite of satellite observations: A case study of application and evaluation for the Indian subcontinent, *Geophys. Res. Lett.*, *33*, L08401, doi:10.1029/2006GL025767.

Papa, F., C. Prigent, C. Jimenez, F. Aires, and W. B. Rossow (2010), Interannual variability of surface water extent at global scale, 1993–2004, *J. Geophys. Res.*, *115*, D12111, doi:10.1029/2009JD012674.

Pielke, R. A. (1984), *Mesoscale Meteorological Modeling*, 767 pp., Academic, New York.

Prigent, C., E. Matthews, F. Aires, and W. B. Rossow (2001a), Remote sensing of global wetland dynamics with multiple satellite data sets, *Geophys. Res. Lett.*, *28*, 4631–4634, doi:10.1029/2001GL013263.

Prigent, C., J. R. Pardo, M. I. Mishchenko, and W. B. Rossow (2001b), Microwave polarized scattering signatures in clouds: SSM/I observations interpreted with radiative transfer simulations, *J. Geophys. Res.*, *106*, 28,243–28,258, doi:10.1029/2001JD900242.

Prigent, C., E. Defer, J. Pardo, C. Pearl, W. B. Rossow, and J.-P. Pinty (2005), Relations of polarized scattering signatures observed by the TRMM Microwave Instrument with electrical processes in cloud systems, *Geophys. Res. Lett.*, *32*, L04810, doi:10.1029/2004GL022225.

Prigent, C., F. Papa, F. Aires, W. B. Rossow, and E. Matthews (2007), Global inundation dynamics inferred from multiple satellite observations, 1993–2000, *J. Geophys. Res.*, *112*, D12107, doi:10.1029/2006JD007847.

Rabin, R. M., S. Stadler, P. J. Wetzel, D. J. Stensrud, and M. Gregory (1990), Observed effects of landscape variability on convective clouds, *Bull. Am. Meteorol. Soc.*, *71*, 272–280.

Raymond, D. J. (1995), Regulation of moist convection over the west Pacific warm pool, *J. Atmos. Sci.*, *52*, 3945–3959.

Rennó, N. O. (1997), Multiple equilibria in a radiative-convective atmosphere, *Tellus*, *49*, 423–438.

Rennó, N. O., K. A. Emanuel, and P. H. Stone (1994a), Radiative-convective model with an explicit hydrologic cycle: 1. Formulation and sensitivity to model parameters, *J. Geophys. Res.*, *99*, 14,429–14,441, doi:10.1029/94JD00020.

Rennó, N. O., P. H. Stone, and K. A. Emanuel (1994b), Radiative-convective model with an explicit hydrologic cycle: 2. Sensitivity to large changes in solar forcing, *J. Geophys. Res.*, *99*, 17,001–17,002, doi:10.1029/94JD01332.

Ringeval, B., N. de Noblet-Ducoudre, P. Ciais, P. Bousquet, C. Prigent, F. Papa, and W. B. Rossow (2010), An attempt to quantify the impact of changes in wetland extent on methane emissions at the seasonal and interannual time scales, *Global Biogeochem. Cycles*, *24*, GB2003, doi:10.1029/2008GB003354.

Rio, C., and F. Hourdin (2008), A thermal plume model for the convective boundary layer: Representation of cumulus clouds, *J. Atmos. Sci.*, *65*, 407–425.

Rio, C., F. Hourdin, J.-Y. Grandpeix, and J.-P. Lafore (2009), Shifting the diurnal cycle of parameterized deep convection over land, *Geophys. Res. Lett.*, *36*, L07809, doi:10.1029/2008GL036779.

Rossow, W. B., and R. A. Schiffer (1999), Advances in understanding clouds from ISCCP, *Bull. Am. Meteorol. Soc.*, *80*, 2261–2288, doi:10.1175/1520-0477.

Taylor, C. M. (2010), Feedbacks on the convection from an African wetland, *Geophys. Res. Lett.*, *37*, L05406, doi:10.1029/2009GL041652.

Tompkins, A. M. (2001), Organization of tropical convection in low vertical wind shears: The role of water vapor, *J. Atmos. Sci.*, *58*, 529–545.

Tompkins, A. M., and G. C. Craig (1999), Sensitivity of tropical convection to sea surface temperature in the absence of large-scale flow, *J. Clim.*, *12*, 462–476.

F. Aires, Estellus, 93 Boulevard de Sébestopol, Paris, F-75002, France.

E. Defer and C. Prigent, Laboratoire d'Etudes du Rayonnement et de la Matière en Astrophysique, CNRS, Observatoire de Paris, 61, Avenue de L'Observatoire, Paris, F-75014, France. (catherine.prigent@obspm.fr)

J.-Y. Grandpeix and N. Rochetin, Laboratoire de Météorologie Dynamique/IPSL/CNRS, Université de Paris VI, 4 Place Jussieu, Paris, F-75005, France.

C. Jimenez, Laboratoire d'Etudes du Rayonnement et de la Matière en Astrophysique, Observatoire de Paris, 61 Avenue de L'Observatoire, Paris, F-75014, France.

F. Papa, Laboratoire d'Etudes en Géophysique et Océanographie Spatiales, IRD, 18 Avenue Edouard Belin, Toulouse, F-31400, France.